

Sequential Activation of Ground Pads Reduces Skin Heating During Radiofrequency Tumor Ablation: *In Vivo* Porcine Results

David J. Schutt, M. Michael Swindle, Kristi L. Helke, Gorka Bastarrika, Florian Schwarz, and Dieter Haemmerich*, *Member, IEEE*

Abstract—Skin burns below ground pads during monopolar RF ablation are increasingly prevalent, thereby hindering the development of higher power RF generators capable of creating larger tumor ablation zones in combination with multiple or new applicators. Our goal was to evaluate reduction in skin temperatures via additional ground pads in an *in vivo* porcine model. Three ground pads placed on the animal's abdomen were activated either simultaneously or sequentially, where activation timing was adjusted to equilibrate skin temperature below each pad. Thirteen RF ablations ($n = 4$ simultaneous at 300 W, $n = 5$ sequential at 300 W, and $n = 4$ sequential at 375 W) were performed for 12 min via two internally cooled cluster electrodes placed in the gluteus maximus of domestic swine. Temperature rise at each pad and burn degree as determined via histology were compared. Ablation zone size was determined via T2-weighted MRI. Maximum temperature rise was significantly higher with simultaneous activation than with either of the sequential activation group (21.4 °C versus 8.1 °C or 9.6 °C, $p < 0.01$). Ablation zone diameters during simultaneous (300 W) and sequential activations (300 and 375 W) were and 6.9 ± 0.3 , 5.6 ± 0.3 , and 7.5 ± 0.6 cm, respectively. Sequential activation of multiple ground pads results in significantly lower skin temperatures and less severe burns, as measured by histological examination.

Index Terms—RF ablation, skin burns, tumor ablation.

I. INTRODUCTION

RF ABLATION has been successfully utilized as a minimally invasive treatment for primary and metastatic liver tumors, as well as tumors in kidney, lung, bone, and adrenal gland tissue [1]–[6]. Since the introduction of RF ablation for tumor treatment, the inability to create large ablation zone volumes without multiple power applications has been a major

limitation. While current commercial systems have allowed the creation of larger coagulation zones (4–6 cm) than initial systems (~1.5 cm), partially due to an increase in maximum generator power (250 versus 50 W), recent studies have shown the possibility of obtaining even larger coagulation zones by using higher power levels (up to 1000 W) [7], [8]. However, it should be noted that not all applicators, currently in clinical use, will benefit from higher power, and new applicators may be required to take advantage of higher power levels.

During RF ablation, dispersive electrodes (or “ground pads”) serve as the return path for applied RF current. Current clinical systems typically employ two or four ground pads placed on both thighs connected in parallel to the RF generator. An important consequence of the use of increased power during RF ablations is the corresponding increase in current density (and thus, heating) at the leading edge of ground pads, since current preferentially flows to the nearest edge of the most proximal pad(s) (the “leading-edge effect”) [9]–[11]. The incidence of skin burns in recent studies ranges from 0.1% to 3.2% for severe skin burns (second or third degree) and from 5% to 33% for first degree burns [12]–[18]. However, two recent studies argue that the incidence of skin burns after RF ablation may be underreported [18], [19]. In addition to monopolar RF devices (i.e., ones with a single electrode requiring ground pads, as described earlier), there are also clinically available multipolar RF devices, where RF current is passed between multiple applicators or electrodes without the need for ground pads [20]. These devices have the advantage that they do not require ground pads, though they are not available in all markets (e.g., not in the U.S.), and the majority of devices in clinical use do employ ground pads.

To date, efforts to reduce ground pad burns have primarily focused on increasing total ground pad area by adding additional pads. However, further improvement to clinical grounding systems in this fashion is impractical because there is no available skin surface to place more than two ground pads per thigh (a pad covers approximately half of the thigh circumference) equidistant from the active electrode (a requirement due to the leading-edge effect). Two RF ablation manufacturers (Angiodynamics and Boston Scientific) have recently incorporated temperature- or current-monitoring features into their commercial ground pads, where RF power is discontinued if temperature or current exceed a threshold. While these features are helpful in reducing the incidence of skin burns, they do not address the fundamental roadblock to higher power RF

Manuscript received July 8, 2009; revised August 26, 2009. First published October 9, 2009; current version published February 17, 2010. This work was supported by the National Institutes of Health under Grant R01 CA118990 and by the Extramural Research Facilities Program of the National Center for Research Resources under Grant C06 RR018823. *Asterisk indicates corresponding author.*

D. J. Schutt is with the Division of Pediatric Cardiology, Medical University of South Carolina, Charleston, SC 29403 USA.

M. M. Swindle and K. L. Helke are with the Department of Comparative Medicine, Medical University of South Carolina, Charleston, SC 29403 USA.

G. Bastarrika is with the Department of Radiology, Clinica Universidad de Navarra, Pamplona 31008, Spain.

F. Schwarz is with the Department of Radiology, Medical University of South Carolina, Charleston, SC 29403 USA.

*D. Haemmerich is with the Division of Pediatric Cardiology, Medical University of South Carolina, Charleston, SC 29403 USA (e-mail: haemmer@usc.edu).

Color versions of one or more of the figures in this paper are available online at <http://ieeexplore.ieee.org>.

Digital Object Identifier 10.1109/TBME.2009.2033385

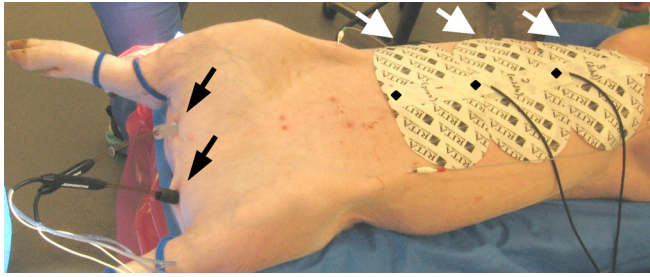


Fig. 1. Typical electrode and ground pad placement. The internally cooled cluster electrodes (black arrows) were placed percutaneously in the center of the left and right gluteal muscles. The ground pads (white arrows) were placed collinearly $\sim 25\text{--}30$ cm from the cluster electrodes. Temperatures were measured at the center of the leading edge of each ground pad (black diamonds).

ablation systems, which is the uneven distribution of heating under ground pads due to the leading-edge effect. Without modification to existing clinical grounding strategies, the incidence of skin burns during RF ablation procedures will likely increase as RF generator power continues to increase.

Two recent studies [21], [22] demonstrated in computer simulations and *ex vivo* gel phantom studies that in the case of three ground pads at different distances from the active electrode, sequential activation of collinear ground pad subsets leads to lower maximum temperatures at the ground pads than if all pads are connected simultaneously. The purpose of this *in vivo* porcine study is to evaluate the performance of a similar sequential activation algorithm in comparison to the grounding method in which all pads are simultaneously activated in an *in vivo* porcine model.

II. MATERIALS AND METHODS

A. Animals, Anesthesia, and Procedures

Preapproval for all animal experiments was obtained from the Institutional Animal Care and Use committee. A total of 13 domestic swine (mean weight approximately 47 kg) were used in this study. Swine were preanesthetized with a combination of injection of ketamine (Ketaset, Ft. Dodge Pharmaceuticals, Overland Park, KS) 22 mg/kg, acepromazine (Acepromazine, Boehringer Ingelheim, Ingelheim, Germany) 1.1 mg/kg, and atropine (Atropine, Abraxis Pharmaceutical Products, Los Angeles, CA) 0.04 mg/kg subcutaneously in the neck. Animals were transported to the operating suite and induced and maintained under general anesthesia with isoflurane (Forane, Baxter Healthcare Corporation Deerfield, IL) 1.5 minimum alveolar concentration (MAC) delivered in 100% oxygen using a gas anesthesia machine. Homeostasis was maintained with IV Lactated Ringers solution 5–10 mL/(kg·h) and monitored with continuous recordings of rectal temperature, pulse oximetry, and ECG [23].

Two internally cooled cluster electrodes (Valleylab ACTC 1525, Boulder, CO) with an exposed length of 2.5 cm were placed in the animal's gluteus maximus (one cluster electrode on each side), approximately equidistant from the leading edge of the proximal ground pad (see Fig. 1). This placement provided

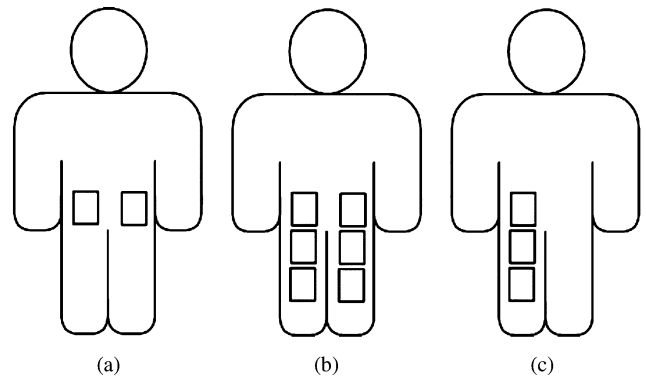


Fig. 2. Diagram of pad placement arrangement. (a) Standard clinical placement with two equidistant pads. (b) Two additional pads are added on each thigh further from the electrode than the original pads (shown in a). (c) Pad placement used in this study, which would correspond to (b) in a clinical setting (i.e., can be translated into humans by using this arrangement on both thighs).

similar distance between proximal ground pad and electrode as in patients. We used two simultaneously activated cluster electrodes because we found in preliminary experiments that one cluster electrode led to rapid impedance rises at the higher power levels (compared to current devices) used in this study, thereby, limiting power levels. The cooling water circulated through the cluster electrodes was kept at $\sim 0^\circ\text{C}$ during all procedures using an ice water bath.

Three ground pads with integral temperature sensors (Thermopads, Angiodynamics, Queensbury, NY) were collinearly placed on each animal's shaved abdomen such that the adhesive region of each pad abutted the adhesive region of the adjacent pad (see Fig. 1), and each pad's built-in temperature sensor was located proximal to the cluster electrodes. A diagram of the rationale behind the ground pad arrangement used in this study is shown in Fig. 2. For the purpose of our study, the proximal pad represented the two or four pads that are currently placed equidistant from the active electrode in clinical RF ablation procedures [see Fig. 2(a)]. The middle and distal pads represent the addition of ground pad area further from the cluster electrodes (since clinically, there is no skin area available for additional equidistant ground pads) to accommodate higher power application [see Fig. 2(c)]; this would be clinically analogous to 6 or 12 total ground pads [three pads on one or both sides of each thigh, Fig. 2(b)].

One RF ablation was performed per animal using one of the ground-pad-activation algorithms described in the Section II-B. After each ablation was completed, the ground pads were removed and pictures were taken of any skin burns. Euthanasia was performed while the animals were still under general anesthesia with a euthanasia solution composed of sodium pentobarbital (Sleepaway, Ft. Dodge Pharmaceuticals, Overland Park, KS) 10 mL intravenous (IV) and potassium chloride (KCl; Hospira, Lake Forest, IL) 10 mL IV. When the ECG indicated death, samples of any discolored or burned skin tissue were excised and placed in 10% neutral buffered formalin for fixation for at least 48 h. The thigh muscle tissues containing the ablation zones were also excised and placed in formalin for at least four weeks to ensure complete fixation of the large samples.

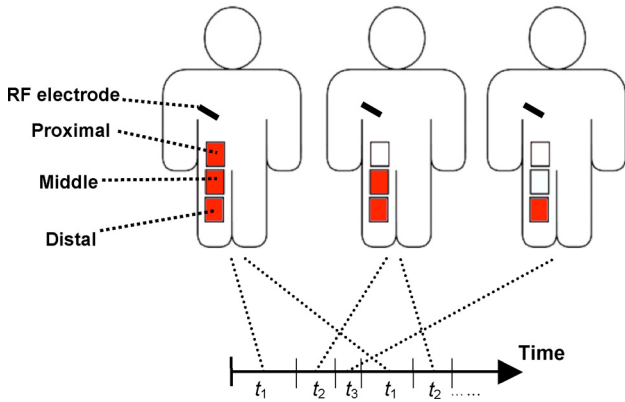


Fig. 3. Timing diagram for sequential activation algorithm of ground pads; pads are labeled proximal, middle, and distal according to location relative to RF electrode. Pads active during each time period t_1 , t_2 , and t_3 are shaded. During power application, skin heating occurs primarily at the leading edge of the activated ground pad that is nearest to the active RF electrode (i.e., the proximal pad during t_1 , the middle pad during t_2 , and the distal pad during t_3). Ratios between t_1 , t_2 , and t_3 were adjusted and total period ($t_1 + t_2 + t_3$) was fixed at 2 s. Typically, $t_1 > t_2 > t_3$ as indicated on the time axis, since active total pad area is largest during t_1 and smallest during t_3 (see, also [22]).

B. Experimental Groups and Ground Pad Control System

A total of 13 ablations (one per animal) were performed in this study. In group 1 (control), four ablations were performed in which all three ground pads were simultaneously activated for the duration of the procedure. In group 2, five ablations were performed with sequential activation of subsets of the ground pads with the same applied power (300 W) as in group 1 [21]. Since in preliminary ablations, we found that sequential activation created smaller ablation zones for a given power level than simultaneous activation (due to lower average current in the former), we also performed four ablations (group 3) with sequential activation and higher power levels (average ~ 375 W) in order to create similar ablation zone size as group 1. A diagram showing the activation cycle for the sequential algorithm used in groups 2 and 3 is shown in Fig. 3.

Fig. 4 shows a block diagram of the ground-pad-activation control system used in this study. A high-power RF generator (500 W, PDX-500, AEL, Fort Collins, CO) supplied RF power at a frequency of 325 kHz (note that this frequency is somewhat lower than the range of 450–500 kHz used in clinical devices; however, this should not affect results significantly). A custom program (Labview, National Instruments, Austin, TX) running on a laptop PC was used to ramp up the applied RF power initially from 50 W to the set power over a period of 30 s, after which constant set power was applied for the remainder of each 12 min ablation. During power application, a data acquisition device (DAQ; 34970 A, Agilent, Santa Clara, CA) continuously measured the applied RF voltage. The control program used this measured voltage and the applied power to calculate impedance and implement an impedance control algorithm; if the calculated impedance exceeded 150% of the initially measured impedance at any point, the program turned off power application for 10 s, and reapplied power at 80% of the previous magnitude. In all groups, the temperature signals from the temperature sensors

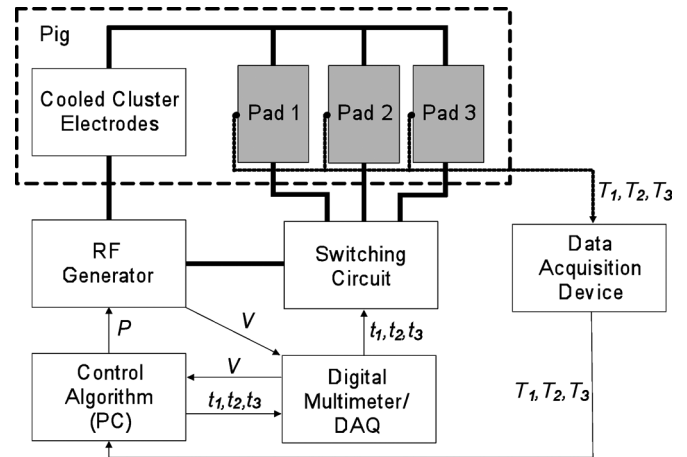


Fig. 4. Diagram of ground pad activation control system. A control algorithm on the PC regulated the generator output power P . A digital multimeter/DAQ measured the applied voltage V and relayed it to the control algorithm, which then calculated the current and impedance. A second DAQ recorded the temperatures (T_1 , T_2 , and T_3) at the leading edge of each ground pad. During the group-1 procedures, all three ground pads were activated for the entire ablation. During the groups 2 and 3 ablations, the control algorithm adjusted the switching periods (t_1 , t_2 , and t_3) via the digital multimeter/DAQ to keep leading-edge temperature equal between pads in a way such that total period ($t_1 + t_2 + t_3$) was kept constant at 2 s.

at the leading edge of each ground pad were filtered for noise removal and recorded at a sampling rate of 100 Hz using a second DAQ (DAQCard-6036E, National Instruments). The magnitude of the applied RF current was calculated by dividing applied power and voltage.

In the group 2 and 3 ablations, the control program continuously updated the activation time periods for each ground pad subset (t_1 , t_2 , and t_3 , see Fig. 3) based on the temperatures recorded by the leading-edge-temperature sensors, with the goal of equilibrating temperatures at each pad. The switching between pad subsets was performed by a custom relay circuit, which interfaced with the control program via digital signals from the Agilent DAQ.

C. Temperature Rise Analysis

The recorded temperature data from each procedure were analyzed to determine the temperature rise at each ground pad. The differences in average temperature rise were compared amongst the three pads using one-way analysis of variance (ANOVA) within each group, and the differences in average temperature rise for each pad between groups 1 and 2 and between groups 1 and 3 were compared using the Mann–Whitney test. Statistical significance was designated as $p < 0.05$, and in any other statistical analysis described later.

D. Histological Analysis of Skin Burns

Histology has long been considered as the gold standard for determining burn depth [24]. It has been shown that burn severity progresses with time (up to 48 h) in deep dermal burns, while superficial burns remain stable [25]. However, all animals were sampled at the same interval postprocedure, which eliminated

TABLE I
SUMMARY OF HISTOLOGICAL SCORING SYSTEM USED TO GRADE SKIN BURNS

Score	Histological features	Clinical burn degree
0	No gross abnormalities	None
1	Vasodilation with sparse perivascular infiltration	1 st
2	Features of 1 plus epidermal necrosis and dense perivascular infiltration	2 nd
3	Features of 2 plus collagen degeneration limited to the upper dermis	2 nd
4	Features of 3 with collagen degeneration in both the upper and mid dermis	2 nd
5	All of the above plus collagen degeneration extending into the hypodermis	3 rd

this variable. After fixation, samples were trimmed, paraffin embedded, sectioned at $\sim 5 \mu\text{m}$, and stained with hematoxylin and eosin (H&E). The resulting slides were then examined in a blinded fashion by a veterinary pathologist, i.e., slides were sequentially numbered starting at the initial experiment, but no information on group or pad location was provided. The sections were graded on a scale modified from the Suzuki scale [26], [27], in which a score between 0 and 5 was assigned to each section. A summary of the scoring methodology is shown in Table I.

A score of 1 corresponds to the clinical assessment of a first degree burn, scores 2–4 correspond to varying levels of a second degree burn, and score 5 is consistent with a third degree burn. Several sections of each sampled area were examined, with the most severe or highest score assigned considered the score for the entire sample. Collagen fibers lose linearity and appear as dense clumps, which is distinct for thermal injury [28]. It is the depth of loss of collagen detail that was used to determine depth of injury.

We performed the Mann–Whitney test between groups 1 and 2 and between groups 1 and 3 at each pad location (proximal, middle, and distal) to determine whether there was a difference in burn score between algorithms. We performed ANOVA within each group to determine whether there was a difference in burn score between different pad locations.

E. Ablation Zone and RF Current Measurement

Ablation zone dimensions were determined via MRI of the fixed muscle samples orthogonal to the RF electrode. Imaging was performed using a 1.5 T MR system (45 mT/m amplitude, 200 T/(m·s) slew rate) (Magnetom Avanto, Siemens Medical Solutions, Erlangen, Germany). A plastic container including the fixed muscle samples was placed in a four-element head

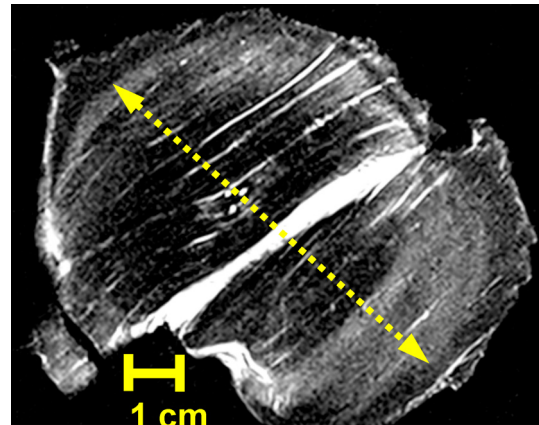


Fig. 5. MR image of ablation zone orthogonal to electrode axis. Location of three-electrode array insertion is visible at the center as three white dots. Dotted arrow represents maximum transverse ablation zone diameter (8.2 cm in this case), and is measured at the boundary of the hyperintense (i.e., bright) rim.

matrix coil. Initial 3-D gradient echo localizers were used to locate samples. Subsequently high-resolution T2-weighted fast spin-echo imaging was performed with the following parameters: echo train length of 14, repetition time (TR): 4000 ms, echo time (TE): 86 ms; two signal averages, field of view (FOV) 100 mm \times 100 mm, matrix 256 \times 256, slice thickness 2 mm, and no interslice gap. The obtained in-plane resolution was 390 μm \times 390 μm . The scans were then manually analyzed to determine the ablation zone maximum transverse diameter and axial diameter by one person in blinded fashion. The ablation zone appears as a hypointense (i.e., dark) region surrounded by a hyperintense (i.e., bright) rim in the MR images (see Fig. 5). A previous study comparing the extents of this region in MR images to histological results demonstrated that the outer boundary of this rim corresponds to the border of necrosis after RF ablation [29]. Axial and maximum transverse ablation zone diameters for groups 1 and 2 and groups 1 and 3 were compared using the Mann–Whitney test. We also reported the measured current during each trial, as well as the impedance values measured 15 s after initial power application.

III. RESULTS

A. Temperature Rise Analysis

In group 1, the temperature rise at the leading edge of the proximal ground pad was significantly higher ($p < 0.001$) than the other two pads after 12 min (see Table II). A graph of the temperatures at the leading edge of each pad for representative ablations in each group is shown in Fig. 6. In groups 2 and 3, the temperature rise was not significantly different between the three pads ($p = 0.5$ and 0.6). The temperature rise at the proximal pad was significantly higher in group 1 than in group 2 or 3, while the temperature rise at the middle and distal pads was significantly higher in groups 2 and 3 than in group 1. The maximum temperature rise after 12 min was significantly higher in group 1 than in group 2 or 3 (21.4°C versus 8.1°C or 9.6°C).

TABLE II
MEASURED INITIAL AND FINAL (AFTER 12 MIN RF ABLATION) TEMPERATURES AT EACH GROUND PAD IN GROUPS 1–3

Group	Proximal pad temperatures, °C		
	Initial	Final	Rise (ΔT)
1	32.2 \pm 0.6	53.6 \pm 4.2 [†]	21.4 \pm 3.6 [†]
2	32.9 \pm 0.5	41.0 \pm 1.0*	8.1 \pm 1.1*
3	32.2 \pm 0.3	41.8 \pm 0.9*	9.6 \pm 1.2*

Group	Middle pad temperatures, °C		
	Initial	Final	Rise (ΔT)
1	33.7 \pm 0.4	35.3 \pm 0.6 [†]	1.6 \pm 0.6 [†]
2	34.0 \pm 0.7	41.7 \pm 1.1*	7.7 \pm 1.0*
3	33.5 \pm 0.3	42.4 \pm 0.8*	8.8 \pm 1.1*

Group	Distal pad temperatures, °C		
	Initial	Final	Rise (ΔT)
1	33.7 \pm 0.1	34.7 \pm 0.5 [†]	1.0 \pm 0.3 [†]
2	34.0 \pm 0.6	41.2 \pm 1.0*	7.2 \pm 0.9*
3	33.4 \pm 0.3	42.3 \pm 0.8*	8.9 \pm 1.0*

Note: Values are means \pm standard deviations.

* $p < 0.05$ (versus group 1).

[†] $p < 0.001$ (group-1 ANOVA).

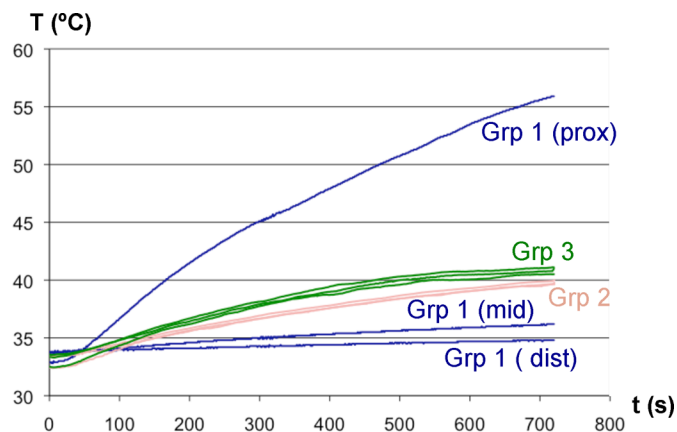


Fig. 6. Temperature profiles for representative experiments in groups 1, 2, and 3. Temperature profiles for proximal, middle, and distal pads are labeled separately for group 1, but not for groups 2 and 3, due to the small difference between pad temperatures.

B. Histological Analysis of Skin Burns

Fig. 8 summarizes the measured skin burn scores. All animals in group 1 had severe burns; third degree [see Fig. 7(b)] burns (score of 5) in three cases and a deep dermal second degree burn (score of 4) in one case. Animals in group 2 had varied burn severities (ranging from 1 to 4) [see Fig. 7(a)]. Individuals in group 3 had more severe burns than those in group 2 (one had severe third degree burn with score of 5, and rest had second degree burns with scores of 2 to 3), although, overall, they were less severe than those in group 1. While there was no significant difference in burn score at the middle pad, the distal pad burns were significantly more severe in group 3 than in

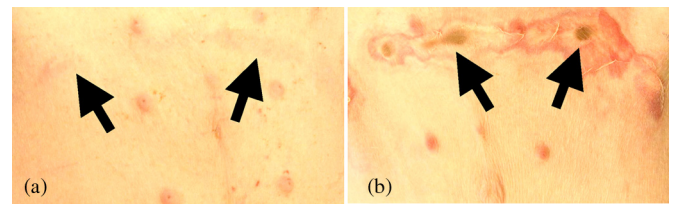


Fig. 7. Gross pathology of skin burns. (a) Animal from group 2: skin shows light reddening (black arrows). This lesion correlated to a score 1 or first degree burn. (b) Animal from group 1: blistering and charring of skin (black arrows) below proximal pad. This lesion correlated to a score 5 or third degree burn.

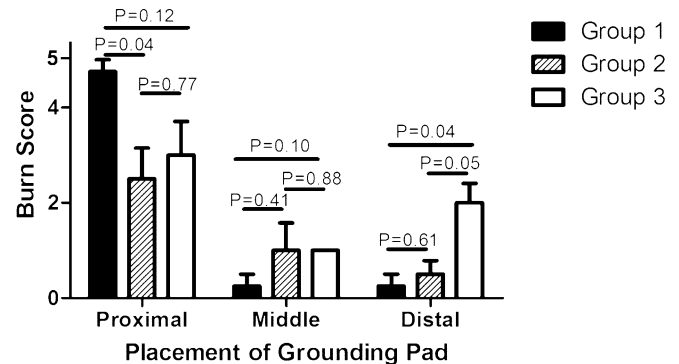


Fig. 8. Graph illustrates mean burn score at each pad for group 1 (simultaneous 300 W), group 2 (sequential 300 W), and group 3 (sequential 375 W). Whiskers represent standard deviations, and p -values for comparison between groups are shown. Comparing the burn scores at pad locations within each respective group, there are significant differences within groups 1 and 3 ($p < 0.0001$ and 0.04), and difference was approaching significance within group 2 ($p = 0.06$).

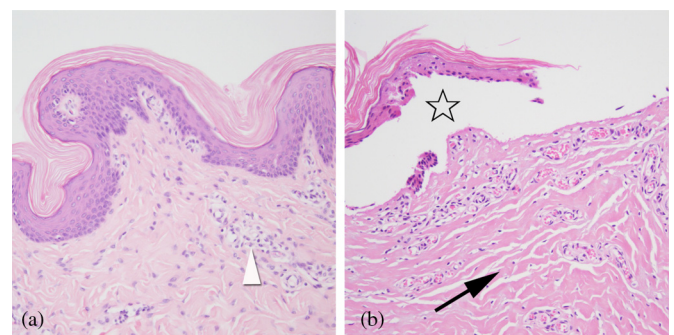


Fig. 9. H&E stained skin samples from region under the ground pad edge. (A, left) Skin from animal in group 2. The epidermis is intact with mild perivascular cellular infiltrate within the upper dermis (white arrowhead). This lesion correlates to a score of 1 or first degree burn. (B, right) Skin below proximal pad from animal in group 1. The epidermis is necrotic and has separated from the dermis (star). Collagen is disrupted and denatured with a hyaline appearance (arrow). This lesion correlates to a score of 5 or third degree burn. 20 \times magnification.

both groups 1 and 2, and the proximal pad in group 1 had a significantly higher score than the proximal pad in group 2 (see Fig. 8). The simultaneous grounding method (group 1) produced severe full-thickness burns extending throughout the dermis into the hypodermis with consistent loss of epidermal layers [see Fig. 9(a)]. In contrast, the sequentially switched algorithm (groups 2 and 3) typically produced only superficial burns with collagen denaturation extending into the superficial

TABLE III
MEASURED ELECTRICAL PARAMETERS DURING 12-MIN RF ABLATIONS

Group	RMS current (A)	Average power (W)	Impedance, all pads (Ω)	Impedance, 2 pads (Ω)	Impedance, 1 pad (Ω)
1	3.4 \pm 0.1	292 \pm 3	31.7 \pm 1.7	NA	NA
2	3.0 \pm 0.1*	292 \pm 7	30.4 \pm 2.0	36.8 \pm 2.6	44.6 \pm 2.2
3	3.7 \pm 0.1*	376 \pm 8*	25.8 \pm 0.8	31.0 \pm 0.7	39.5 \pm 0.5

Note: Values are means \pm standard deviations. All impedance values represent initial impedance (15 s).

* $p < 0.05$ (versus group 1).

dermis [see Fig. 9(b)]. The epidermis was consistently affected in groups 2 and 3, with nuclear shrinkage and condensation, but not to the degree observed in group 1, which exhibited complete loss of cellular detail and separation of the epidermis from the dermis.

The comparison of the results to an additional control group, where pads are applied for 12 min without any application of RF energy, and subsequent histological skin analysis may be of interest. However, considering that in group 1 the distal pad reached a maximum average measured temperature of 34.7 °C, that these pads had burn scores close to zero, and that no skin reddening (a sign of first degree burn) was visible after the procedure below these pads, it is likely that these data are similar to results one would get for pads without power application.

C. Electrical Parameters and Ablation Zone Dimensions

Resection of each ablation zone in its entirety was difficult due to the large size of the zones and the heterogeneity of muscle tissue. Therefore, we only included the measurements of 15 ablation zones ($n = 4, 4,$ and 7 for groups 1, 2, and 3 respectively) in our statistical analysis of their dimensions.

The average applied power was significantly higher in group 3 than in group 1 ($p < 0.05$), but not different between groups 1 and 2 ($p = 0.99$). The rms current applied in group 2 was significantly lower than in group 1, and higher in group 3 than groups 1 and 2. Correspondingly, the maximum transverse diameter of the group-2 ablation zones was also significantly lower than group 1 (see Table IV). The higher rms current applied in the group-3 ablations resulted in larger maximum transverse diameters than group 1 (see Table IV), with the difference approaching statistical significance ($p = 0.05$). There was no significant difference in the axial diameters of the ablation zones between the three groups. There was also no significant difference in initial impedance (with all three pads activated) between the three groups ($p = 0.07$) (see Table III). An impedance rise was observed during power application in one case in groups 1 and 2 and in two cases in group 3.

IV. DISCUSSION

Higher RF generator power will likely be required in future monopolar RF tumor ablation systems to create larger ablation zones that fully treat large tumors. Two recent studies showed that even with some current commercial RF electrodes, larger ablation zones could be created if higher RF power was used [7], [8]. However, existing ground pad technology is currently a limiting factor for further increase in RF generator power

TABLE IV
MEASURED ABLATION ZONE DIMENSIONS FROM 12 MIN RF ABLATIONS

Group	n	Maximum transverse diameter (cm)	Axial diameter (cm)
1	4	6.9 \pm 0.3	5.6 \pm 0.8
2	4	5.6 \pm 0.3*	5.6 \pm 0.5
3	7	7.5 \pm 0.6*	6.5 \pm 0.8

Note: Values are means \pm standard deviations.

* $p < 0.05$ (versus group 1).

* $p = 0.12$ (versus group 1).

for clinical tumor ablation devices. It should be noted that there are also multipolar RF devices available, where multiple electrodes (on a single, or on multiple applicators) are inserted into the tumor, where RF current is passed between these multiple electrodes. Since these devices do not require ground pads, skin burns are not a concern. There are clinical multipolar RF devices available in some markets, though the majority of procedures are performed with monopolar devices that do require ground pads.

One potential way to reduce skin heating compared to current clinically used ground pad methodology [see Fig. 2(a)] is increasing the ground pad area, or as employed in the present study, increasing the number of ground pads [see Fig. 2(b)]. We compared two methodologies of activating these additional pads: 1) simultaneous activation, where all pads are active and 2) sequential activation via algorithm shown in Fig. 3. Note that while in the animal study, only three pads were applied [equivalent to the arrangement on one thigh, Fig. 2(c)], the results can be extended to multiple thighs as clinically used, i.e., three pads would be placed on each thigh [see Fig. 2(b)] and activated according to the algorithm described earlier.

In this study, we performed ablations with up to 375 W for 12 min, which is considerably higher power than currently used clinically (200–250 W). Three ground pads with integrated temperature sensors were placed in a collinear arrangement approximately 30 cm from the active electrodes [see Figs. 1 and 2(c)]. As may be expected, the simultaneous activation of three collinear ground pads (i.e., at varied distances from the active electrode) results in heating of primarily the proximal pad, where the majority of applied current is dispersed with likely little benefit of the two additional pads. Therefore, the arrangement in Fig. 2(b) does not provide significant benefit over the current clinically used arrangement in Fig. 2(a). The goal of this study was to investigate whether the use of a sequential activation algorithm with this ground pad configuration could reduce skin heating during ablation in comparison to the simultaneous activation of all pads. The sequential activation algorithm resulted in considerably lower maximum skin temperature at the leading edge of the pads at both power levels (see Table II), and significantly reduced the incidence and severity of skin burns (see Figs. 8 and 9). Simultaneous activation consistently results in severe, full-thickness skin burns at the proximal pad due to the leading-edge effect (i.e., most electrical current and resulting heating is produced at the ground pad edge closest to the RF electrode), while sequential activation typically resulted in superficial burns only.

Leading-edge temperatures at all three pads were successfully equilibrated in the group 2 and 3 ablations (see Table II,

Fig. 6), whereas in the group-1 ablations, only the proximal pad experienced significant heating (see Table II, Fig. 6) as expected. However, burn score was not equivalent between each pad within groups 2 and 3. This may be due to variance in the temperature profile along the leading edge of each pad based on the distance from the active electrode; additional temperature sensors near the pad corners, where the most severe burns occurred [see Fig. 7(b)], may allow for better control during sequential activation.

During the time periods when only one or two pads were activated with the sequential algorithm (activation times t_2 and t_3 in Fig. 3), the impedance increased (see Table III). This increase occurred because the distance between the cluster electrodes and the closest activated ground pad increased, and because the overall activated ground pad area was reduced (see Table III). This is also the reason why typically the switching period lengths were ranked such that $t_1 > t_2 > t_3$ (see [22] for further details).

During ablation, the total available RF power produces intended tissue heating around the RF electrode, as well as unintended skin heating below the pads. With reduced ground pad area in group 2 compared to group 1, more power was deposited below the pads and less power deposited around the RF electrode. This resulted in smaller ablation zone diameters in group 2 versus group 1 (5.6 versus 6.9 cm) (see Table IV). To account for the effect of increased impedance during sequential activation on ablation zone size, we applied higher power (average ~ 375 W, Table III), using the sequential activation algorithm in group 3. The higher applied power used in group 3 led to larger ablation zone diameters than group 1 (7.3 versus 6.9 cm, $p = 0.05$) (see Table IV), while still significantly lowering maximum ground pad temperature and reducing burn severity, although this difference did not reach significance ($p = 0.12$, Fig. 9). Likely, skin temperatures in group 3 were close to the threshold required for third degree burns (burn score 5); therefore, even though temperatures were considerably higher in group 1, the difference in burn score was smaller than the temperature differences would suggest, since once the burn score has reached maximum value, further increase in temperature do not increase burn score.

Additional optimization of the size of multiple pads and their distance from the RF electrode may provide further reduction in skin heating during application of the sequential algorithm [22]. Note that instead of multiple pads, a single pad with multiple isolated pad areas would achieve the same affect while likely being more practicable.

We had investigated the potential benefit of sequential activation of multiple ground pads in two recent studies, where we employed computational heat-transfer modeling to determine tissue temperatures [21], [22]. While absolute temperature values in the computer simulations are not directly comparable to the present study due to differences in applied RF energy and pad size, qualitatively the *in vivo* results presented here are in agreement with the computational modeling studies with considerably smaller tissue temperatures with sequential activation. In computer simulations, temperature increase was reduced by approximately two times [22], which is in the same range that was observed here (see Table II), i.e., in this case, computational

models allowed testing of our hypothesis and, thereby, reduced the need for animal studies.

The limitations of this study include the reduced number of measurements obtained due to difficulties in excising the ablation zones, which may affect the accuracy of our comparisons. Additionally, as noted previously, the highest temperatures at each pad during the ablations may not have occurred at the location of the temperature sensor. Finally, it is important to note that the results presented in this study could vary during clinical application due to differences in skin and fat layer thickness, perfusion, and other parameters.

V. CONCLUSION

The benefit of using multiple ground pads on each thigh during monopolar RF ablation was investigated *via* two different activation algorithms. While simultaneous activation provides a little benefit, sequential activation takes advantage of the additional pad area and, considerably, reduces skin heating. In addition, the sequential activation algorithm would eliminate the need to place all ground pads equidistant from the active RF electrode, since pad activation times are adjusted to keep all pads at the same temperature. This method would, therefore, allow the placement of ground pads on currently unused areas of the patient's skin (e.g., back, or additional pads on thighs corresponding to the arrangement in the current study), thereby, reducing maximum skin temperatures and skin burn incidence, and/or allowing the use of higher RF generator power.

REFERENCES

- [1] M. A. Farrell, W. J. Charboneau, D. S. DiMarco, G. K. Chow, H. Zincke, M. R. Callstrom, B. D. Lewis, R. A. Lee, and C. C. Reading, "Imaging-guided radiofrequency ablation of solid renal tumors," *AJR Amer. J. Roentgenol.*, SC, vol. 180, no. 6, pp. 1509–1513, Jun. 2003.
- [2] D. A. Gervais, F. J. McGovern, R. S. Arellano, W. S. McDougal, and P. R. Mueller, "Renal cell carcinoma: Clinical experience and technical success with radio-frequency ablation of 42 tumors," *Radiology*, vol. 226, no. 2, pp. 417–424, Feb. 2003.
- [3] W. W. Mayo-Smith and D. E. Dupuy, "Adrenal neoplasms: CT-guided radiofrequency ablation—preliminary results," *Radiology*, vol. 231, no. 1, pp. 225–230, Apr. 2004.
- [4] Z. Neeman and B. J. Wood, "Radiofrequency ablation beyond the liver," *Tech. Vasc. Interv. Radiol.*, vol. 5, no. 3, pp. 156–163, Sep. 2002.
- [5] D. I. Rosenthal, F. J. Hornicek, M. Torriani, M. C. Gebhardt, and H. J. Mankin, "Osteoid osteoma: Percutaneous treatment with radiofrequency energy," *Radiology*, vol. 229, no. 1, pp. 171–175, Oct. 2003.
- [6] B. J. Wood, J. Abraham, J. L. Hvizda, H. R. Alexander, and T. Fojo, "Radiofrequency ablation of adrenal tumors and adrenocortical carcinoma metastases," *Cancer*, vol. 97, no. 3, pp. 554–560, Feb. 1, 2003.
- [7] C. L. Brace, P. F. Laeseke, L. A. Sampson, T. M. Frey, R. Mukherjee, and F. T. Lee, Jr., "Radiofrequency ablation with a high-power generator: Device efficacy in an *in vivo* porcine liver model," *Int. J. Hyperthermia*, vol. 23, no. 4, pp. 387–394, Jun. 2007.
- [8] S. A. Solazzo, M. Ahmed, Z. Liu, A. U. Hines-Peralta, and S. N. Goldberg, "High-power generator for radiofrequency ablation: Larger electrodes and pulsing algorithms in bovine *ex vivo* and porcine *in vivo* settings," *Radiology*, vol. 242, no. 3, pp. 743–750, Mar. 2007.
- [9] S. N. Goldberg, L. Solbiati, E. F. Halpern, and G. S. Gazelle, "Variables affecting proper system grounding for radiofrequency ablation in an animal model," *J. Vasc. Interv. Radiol.*, vol. 11, no. 8, pp. 1069–1075, Sep. 2000.
- [10] V. T. Krasteva and S. P. Papazov, "Estimation of current density distribution under electrodes for external defibrillation," *Biomed. Eng. Online*, vol. 1, p. 7, Dec. 16, 2002.

- [11] K. S. Tan and I. Hinberg, "Temperature distribution beneath pediatric electrosurgical dispersive electrodes: A model study," *Biomed. Instrum. Technol.*, vol. 27, no. 6, pp. 506–513, Nov./Dec. 1993.
- [12] R. J. Bleicher, D. P. Allegra, D. T. Nora, T. F. Wood, L. J. Foshag, and A. J. Bilchik, "Radiofrequency ablation in 447 complex unresectable liver tumors: Lessons learned," *Ann. Surg. Oncol.*, vol. 10, no. 1, pp. 52–58, Jan./Feb. 2003.
- [13] B. J. Bowles, J. Machi, W. M. Limm, R. Severino, A. J. Oishi, N. L. Furumoto, L. L. Wong, and R. H. Oishi, "Safety and efficacy of radiofrequency thermal ablation in advanced liver tumors," *Arch. Surg.*, vol. 136, no. 8, pp. 864–869, Aug. 2001.
- [14] T. Livraghi, L. Solbiati, M. F. Meloni, G. S. Gazelle, E. F. Halpern, and S. N. Goldberg, "Treatment of focal liver tumors with percutaneous radiofrequency ablation: Complications encountered in a multicenter study," *Radiology*, vol. 226, no. 2, pp. 441–451, Feb. 2003.
- [15] S. Mulier, P. Mulier, Y. Ni, Y. Miao, B. Dupas, G. Marchal, I. D. Wever, and L. Michel, "Complications of radiofrequency coagulation of liver tumours," *Br. J. Surg.*, vol. 89, no. 10, pp. 1206–1222, Oct. 2002.
- [16] H. Rhim, "Complications of radiofrequency ablation in hepatocellular carcinoma," *Abdom. Imag.*, vol. 30, no. 4, pp. 409–418, Jul./Aug. 2005.
- [17] K. Steinke, S. Gananadha, J. King, J. Zhao, and D. L. Morris, "Dispersive pad site burns with modern radiofrequency ablation equipment," *Surg. Laparosc. Endosc. Percutan Tech.*, vol. 13, no. 6, pp. 366–371, Dec. 2003.
- [18] T. F. Wood, D. M. Rose, M. Chung, D. P. Allegra, L. J. Foshag, and A. J. Bilchik, "Radiofrequency ablation of 231 unresectable hepatic tumors: Indications, limitations, and complications," *Ann. Surg. Oncol.*, vol. 7, no. 8, pp. 593–600, Sep. 2000.
- [19] J. Machi, "Prevention of dispersive pad skin burns during RFA by a simple method," *Surg. Laparosc. Endosc. Percutan Tech.*, vol. 13, no. 6, pp. 372–373, Dec. 2003.
- [20] S. Clasen, D. Schmidt, A. Boss, K. Dietz, S. M. Krober, C. D. Claussen, and P. L. Pereira, "Multipolar radiofrequency ablation with internally cooled electrodes: Experimental study in ex vivo bovine liver with mathematic modeling," *Radiology*, vol. 238, no. 3, pp. 881–890, Mar. 2006.
- [21] D. Haemmerich and D. J. Schutt, "Sequential activation of multiple grounding pads reduces skin heating during radiofrequency tumor ablation," *Int. J. Hypertherm.*, vol. 23, no. 7, pp. 555–566, 2007.
- [22] D. J. Schutt and D. Haemmerich, "Sequential activation of a segmented ground pad reduces skin heating during radiofrequency tumor ablation: Optimization via computational models," *IEEE Trans. Biomed. Eng.*, vol. 55, no. 7, pp. 1881–1889, Jul. 2008.
- [23] M. M. Swindle, *Swine in the Laboratory: Surgery, Anesthesia, Imaging and Experimental Techniques*. Boca Raton, FL: CRC Press, 2007.
- [24] S. Sevitt, *Burns: Pathology and Therapeutic Applications*. London: Butterworth, 1957.
- [25] A. Papp, K. Kiraly, M. Harma, T. Lahtinen, A. Uusaro, and E. Alhava, "The progression of burn depth in experimental burns: A histological and methodological study," *Burns*, vol. 30, no. 7, pp. 684–690, Nov. 2004.
- [26] F. X. S. Heredero, C. Hamann, J. M. O. Martin, C. R. Arias, and S. C. Menchero, "Experimental burn models," *Ann. Burns Fire Disasters*, vol. IX, no. 2, pp. 96–100, Jun. 1996.
- [27] T. Suzuki, T. Hirayama, K. Aihara, and Y. Hirohata, "Experimental studies of moderate temperature burns," *Burns*, vol. 17, no. 6, pp. 443–451, Dec. 1991.
- [28] S. M. Srinivas, J. F. de Boer, H. Park, K. Keikhanzadeh, H. E. Huang, J. Zhang, W. Q. Jung, Z. Chen, and J. S. Nelson, "Determination of burn depth by polarization-sensitive optical coherence tomography," *J. Biomed. Opt.*, vol. 9, no. 1, pp. 207–212, Jan./Feb. 2004.
- [29] M. S. Breen, R. S. Lazebnik, M. Fitzmaurice, S. G. Nour, J. S. Lewin, and D. L. Wilson, "Radiofrequency thermal ablation: Correlation of hyperacute MR lesion images with tissue response," *J. Magn. Reson. Imag.*, vol. 20, no. 3, pp. 475–486, Sep. 2004.



David J. Schutt was born on April 2, 1977, in Wyandotte, MI. He received the B.S. degree from the Department of Electrical Engineering and the M.S. degree from the Department of Biomedical Engineering, University of Wisconsin, Madison, in 2000 and 2005, respectively.

He is currently a Research Specialist with the Division of Pediatric Cardiology, Medical University of South Carolina, Charleston. His research interests include tumor ablation, cardiac ablation, and biomedical instrumentation.



M. Michael Swindle received the B.S. and D.V.M. degrees from Texas A&M University, College Station, in 1968 and 1969, respectively.

He served the U.S. Army and later completed a residency in pathobiology and comparative medicine from the Johns Hopkins University, Baltimore, MD, from 1979 to 1981. He is a Diplomate of American College of Laboratory Animal Medicine and European College of Laboratory Animal Medicine. From 1981 to 1985, he was an Assistant Professor in the Departments of Surgery and Comparative Medicine, Johns Hopkins School of Medicine, Johns Hopkins University, where he was a Supervisor of the Surgical Research Labs. Since 1985, he has been a Professor and the Chairman with the Department of Comparative Medicine, Medical University of South Carolina, where has also been a Professor with the Department of Surgery. His current research interests include porcine surgical models.



Kristi L. Helke received the Veterinary degree in 2000 from the University of Wisconsin-Madison and the Ph.D. degree in pathobiology with an emphasis on neurodegeneration from Johns Hopkins University, Baltimore, MD.

She was subsequently selected as a Postdoctoral Fellow in veterinary pathology at Johns Hopkins University, where she has published several papers on investigating mechanism of disease. These studies range from the development of new models to emulate specific diseases to changing the course of experimental disease in defined models. She is currently an Assistant Professor with the Department of Comparative Medicine, Medical University of South Carolina, Charleston.



Gorka Bastarrika received the M.D. degree from the University of Navarre, Pamplona, Spain, in 1998, from where he completed the postgraduate medical clinical training in radiology in 2003.

He is currently an attending Clinician with the University of Navarre. He has also completed a research scholarship on noninvasive cardiac imaging at the Medical University of South Carolina, Charleston.

Florian Schwarz, photograph and biography not available at the time of publication.



Dieter Haemmerich (S'00–M'02) received the Ph.D.B.M.E. degree from the University of Wisconsin-Madison, Madison, Wisconsin, in 2001, and the Ph.D.E.E. degree from the Vienna University of Technology, Vienna, in 2003.

He is currently an Associate Professor of pediatric cardiology with the Medical University of South Carolina, Charleston, and Adjunct Faculty of Bioengineering, Clemson University, Clemson, SC. His research interests include thermal ablation, biomedical instrumentation, measurement of thermal and dielectric tissue properties, and computational modeling of bioheat transfer problems and targeted drug delivery.